Colloids and Surfaces B: Biointerfaces 230 (2023) 113506

Contents lists available at ScienceDirect

Colloids and Surfaces B: Biointerfaces

journal homepage: www.elsevier.com/locate/colsurfb

The bio-functionalized membrane loaded with Ta/WH nanoparticles promote bone regeneration through neurovascular coupling

Kai Zhang [a,b], Hongkun Hu [a,b], Yan Sun [a,b], Jiangyu Nan [a,b], Wenbin Liu [d,*], Pengfei Lei [a,b,c,**], Yihe Hu [a,b,c,**]

[a] Department of Orthopedic Surgery, National Clinical Research Center for Geriatric Disorders, Xiangya Hospital, Central South University, Changsha, China
[b] Hunan Engineering Research Center of Biomedical Metal and Ceramic Implants, Changsha, China
[c] Department of Orthopedics, The First Affiliated Hospital, Medical College of Zhejiang University, Hangzhou, China
[d] Department of Orthopaedics, The Third Xiangya Hospital Central South University, 138 Tongzipo Road, Changsha, Hunan China.

ARTICLE INFO

Keywords:
Electrospinning
Tantalum
Bone repair
Angiogenesis
Neurogenesis

ABSTRACT

Electrospinning technology, as a novel approach, has been extensively applied in the field of tissue engineering. Nanofiber membranes prepared by electrospinning can effectively mimic the structure and function of natural bone matrix, providing an ideal scaffold for attachment, proliferation, and differentiation of bone cells while inducing osteogenic differentiation and new bone formation. However, it lacks bioactivities such as osteoinduction, angiogenesis and the ability to promote nerve regeneration. In the presence of complex critical bone defects, a single component electrospun membrane often fails to suffice for bone repair needs. Based on this, we prepared a biofunctionalized membrane loaded with Tantalum(Ta)/Whitlockite(WH) nanoparticles (poly-ε-caprolactone (PCL)/Ta/WH) in order to promote high-quality bone defect repair through neurovascular coupling effect. According to the results of *in vitro* and *in vivo* experiments, the early Mg^{2+} release of WH can effectively increase the local nerve and vascular density, and synergize with Tantalum nanoparticles (TaNPs) to create a rich nerve-vascular microenvironment. This allows the PCL/Ta/WH membrane to repair bone defects in multiple dimensions and achieve high-quality repair of bone tissue, providing new solutions for the treatment of critical bone defects in clinical.

1. Introduction

The treatment of large bone defects is still a major challenge in clinical, caused by trauma, infection, tumors and other diseases [1]. Although autologous bone transplantation is the gold standard for treatment, drawbacks such as insufficient sources and infection in the supply area hamper its application. Allogeneic bone also faces problems such as immune rejection[2,3]. In order to overcome these limitations, researchers are increasingly focusing on how to develop new artificial bone repair materials to replace autologous and allogeneic bones to achieve high-quality repair of large bone defects.

At present, artificial bone repair materials are roughly divided into several categories, including metals (Ti, Ta),ceramics (TCP, HA), and polymers (PCL, PLA). These materials are widely used due to their wide sources, good biocompatibility, osteoinduction, no rejection reaction, etc[4]. Rapid advancements in the fields of materials science and tissue engineering have facilitated the development and accomplishment of superior composite systems for repairing or reconstructing damaged bone tissue[5,6]. To achieve this goal, it is necessary to construct a suitable material system which, simulates the microstructure and function of natural bone tissue, promotes the proliferation, migration and differentiation of functional cells (such as osteoblasts, vascular endothelial cells, and nerve cells) in the bone defect area. Ultimately, efficient repair of bone tissue can be achieved.

Natural bone tissue is a complex multi-level system composed of two parts (organic and inorganic). The organic part is mainly collagen, and the inorganic part is mainly crystals of calcium carbonate and calcium phosphate[7–9]. Collagen and inorganic crystals are intertwined to form a composite structure with high strength and toughness[10,11]. Electrospinning, as a new method widely used in tissue engineering, exerts

* Corresponding author.
** Corresponding authors at: Department of Orthopedic Surgery, National Clinical Research Center for Geriatric Disorders, Xiangya Hospital, Central South University, Changsha, China.
E-mail addresses: liuwenbin1995@126.com (W. Liu), leipengfei@zju.edu.cn (P. Lei), xy_huyh@163.com (Y. Hu).

https://doi.org/10.1016/j.colsurfb.2023.113506
Received 13 June 2023; Received in revised form 27 July 2023; Accepted 5 August 2023
Available online 7 August 2023

high-voltage electrostatic fields to stretch polymers in solutions or forge them into nanometer or micrometer fibers[12]. It can effectively simulate the structure and function of natural bone matrix, provide a good scaffold for the attachment, proliferation and differentiation of bone cells, induce osteogenic differentiation and new bone formation[13,14]. At present, most of the substrate materials used for electrospinning are polymers (such as polycaprolactone (PCL); polyethylene glycol (PEG); poly lactic-co-glycolic acid (PLGA); polyvinylpyrrolidone (PVP))[15]. Although it exhibits favorable biocompatibility and degradability, it lacks bioactivity such as osteoinduction and the ability to promote nerve regeneration[16]. In the case of complex critical bone defects, a single electrospinning membrane may not suffice to meet the requirements for effective bone repair.

Repair of bone defects is a highly complex process that requires the participation of stem cells, blood vessels, nerves and other factors[17]. Stem cells, as seed cells, have the ability to self-renew and differentiate into multiple cell types[18]. They can be used in tissue engineering and regenerative medicine, providing new possibilities for the treatment of various diseases and injuries[18,19]. There exists a significant amount of literature has demonstrated the critical role of neovascularization in bone repair, as the network of new blood vessels within the defect area can more effectively supply essential nutrients and oxygen to promote tissue regeneration, while activating osteoprogenitor cells and osteoblasts to promote the synthesis and mineralization of bone matrix [20–22]. It is worth noting that bone tissue is primarily innervated by a dense sensory nerve network, with nerve cells capable of secreting various neurotrophic factors such as nerve growth factor (NGF), brain-derived neurotrophic factor (BDNF), and neurofilament (NF)[23]. These factors can stimulate the proliferation, differentiation and mineralization of osteoblasts, enhance the formation and calcification of bone matrix[24]. At the same time, nerve cells can also establish a nerve-bone junction (NBO) with osteoblasts to transmit mechanical and electrical signals, regulate bone remodeling and adapt to mechanical stress[25,26]. Tissue-engineered bone neuralization is considered a promising strategy that can effectively overcome the challenges of vascularization and nerve regeneration in the central area of "critical size bone defects" that traditional tissue engineering scaffolds cannot handle[27–29]. Therefore, how to accurately regulate the functional differentiation of nerves, blood vessels and stem cells is a key factor in achieving high-quality repair of bone defects.

According to the our previous reports, TaNPs as osteoinduction enhancers can effectively improve the osteogenic performance of polymers and have the potential to be used as local bone immune microenvironment regulators[30]. As a natural mineralization material, WH has been proven to effectively promote the formation of local nerve and vascular networks in natural bone tissue, with its content second only to HA in natural bones[31–33]. Based on this, we prepared a bio-functionalized membrane loaded with Ta/WH nanoparticles to promote high-quality repair of bone defects through the nerve-vascular coupling effect. The early Mg^{2+} release of WH can effectively increase the local nerve and vascular density, and synergize with tantalum nanoparticles to create a rich nerve-vascular microenvironment. This allows the PCL/Ta/WH membrane to repair bone defects in multiple dimensions and achieve high-quality repair of bone tissue, providing new solutions for the treatment of critical bone defects in clinical.

2. Materials and methods

2.1. Preparation of PCL-Ta-WH electrospun nanofiber membrane

Ta NPs were synthesize by Dk Nanotechnology Co., Ltd. (Beijing Dk Nanotechnology Co., Ltd., China, size = 50 nm), and WH NPs were synthesized by a hydroxide precipitation method using calcium hydroxide ($Ca(OH)_2$), magnesium hydroxide ($Mg(OH)_2$), and phosphoric acid (H_3PO_4) [all materials were purchased from China National Pharmaceutical Group Chemical Reagent Co., Ltd.] through a water-based system. The electrospinning technique was employed to fabricate PCL/Ta/WH nanofibrous membranes. In simple terms, PCL was dissolved in 2,2,2-trifluoroethanol, and TaNPs were added to the PCL solution at 5% (w/v) and WH at 15% (w/v). The mixture was sonicated for 30 mins to uniformly disperse the nanoparticles. Then it was loaded into a 10 ml syringe and waited for electrospinning. The solution system in the syringe flowed in an electric field between the needle tip (+5kv) and aluminum foil (−2 kV), 0.5 ml/h. Pure PCL film and PCL/Ta film were used as controls for this study. The materials used in the biological experiments of this study were sterilized with ethylene oxide.

2.2. Materials characterization

Surface appearance: The prepared PCL, PCL/Ta, and PCL/Ta/WH membranes were cut into 1 × 1 cm size, sprayed with gold, and then observed for morphology using SEM under an acceleration voltage of 20 kV. The existence of each element in the membrane was confirmed by energy dispersive analysis (EDS). **XRD test**: The membrane was subjected to phase analysis by X-ray diffraction(XRD) analyzer under the following test conditions:copper target (λ = 0.15418 nm), tube voltage of 40 kV, tube current of 25 mA, scanning speed of 0.5°/min, and scanning range of 5° ~ 130°. **Water contact angle:** After cutting the nanofiber membrane into 1 × 1 cm size, use the contact angle measuring instrument (OSA200-B) to test the water contact angle of each fiber membrane. Each sample is tested three times and the average value is calculated. **Mechanical test:** Using the stretching experimental device to measure the mechanical properties, the length of the spinning film is 1 cm, the displacement speed is 5 cm/min, and the data such as load, displacement, and stress are recorded. The experimental results are analyzed, and the stress-strain curve of the material is calculated and compared with the theoretical value or standard value. **Ions release:** Immerse a 1 × 1 cm membrane in 5 ml ddH2O solution, and take 200 μl for ICP detection of Mg^{2+} concentration on days 1, 3, 5, 7, 10, and 14.

2.3. Cellular compatibility

Rat aortic endothelial cells (RAECs), bone marrow mesenchymal stem cells (BMSCs), and rat pheochromocytoma cell lines (PC-12) was purcgased from the Chinese Tissue Culture Collection(CTCC-001-0057). These three types of cells represent the cell types of the vascular, skeletal, and nervous systems, respectively, and can simulate the interaction between biomaterials and medical devices and different parts of the human body. RAECs and PC-12 were cultured in DMEM (Basalmedia) + 10% FBS + 1% Penicillin-Streptomycin Solution (P/S, BioChannel Biological Technology Co, Ltd.), BMSCs were cultured in α-MEM (VivaCell, Shanghai, China) + 10% FBS + 1% P/S. The environmental conditions were 37 ℃ and 5% CO_2. The following experiments were used to detect the biocompatibility of RAECs, BMSCs, and PC-12 cells: cell proliferation assay: 5000/well cells were seeded in a 48-well plate (Guangzhou Jet Bio-Filtration Co., Ltd. (stock code: 688026)), and cell activity was detected on the first and third days. 300 μl of 10% concentration CCK8 medium was added to each well, and after incubation at 37 ℃ and 5% CO_2 for 1 h, the absorbance at 450 nm of each well was measured to determine the toxicity of the sample extract on cells. Cell viability assay: 5000/well cells were seeded in a 48-well plate. On the first and third days, Calcein-AM/PI staining was used, and photos were taken under a fluorescence microscope. The FBS was purchased from CellMax Co., Ltd. (China). The Glass Bottom Cell Culture Dish for confocal microscope photography was purchased from SORFA Life Science (China). The Penicillin-Streptomycin Solution was purchased from BioChannel Biological Technology Co, Ltd.

2.4. In vitro studies

Tube formation experiment: The angiogenic properties of the nanofibrous membranes were assessed using a tube formation assay.

Matrigel was placed at 4 ℃ overnight and thawed. The pipette tips and 48-well plate were pre-cooled on ice. All operations during the plate laying were performed on ice. 110 μl of matrix gel was injected into each well, placed at 4 ℃ to make the matrix gel flow flat, and then placed at 37 ℃ for 30 mins to make it gel. RAECs with a density of 2.5×10^4/well were seeded in the plate. After 4 h, inverted fluorescence microscopy (Nikon TE 2000-U, Nikon Instruments Inc.) was used to observe the cells. Then Calcein-AM staining was performed for 10 min and photos were taken. Five ROIs were randomly selected from each well for statistical analysis. The matrigel was purchased from absin Biotechnology Co., LTD (stock code:abs-9490). **Osteogenic differentiation experiment:** The effect of the sample on the osteogenic differentiation ability of BMSCs was measured. BMSCs with a density of 1×10^4/cm^2 were seeded on a membrane with a diameter of 8 mm and cultured in osteogenic induction medium (composition) for 5 days. After cell fixation for 30 mins on day 5, ALP detection reagent kit staining was performed. Sirius staining was performed on days 7 and 14, and ARS staining was performed on days 14 and 21. Semi-quantitative detection was performed using a Bio-Tek enzyme-linked immunosorbent assay reader. The absorbance of Sirius and ARS staining were measured at 540 nm and 565 nm, respectively. **Neurogenesis research study**: Transwell experiment: RSCs cells with a density of 3×10^4/well were seeded in the Transwell chamber, and a membrane with a diameter of 8 mm was placed in the lower chamber. The cells and nanofiber membranes were co-cultured in a cell incubator for 24 h. After fixation with 4% PFA for 30 min, PBS (Bioss) was washed three times, crystal violet staining was performed for 30 min, and then photos were taken under an inverted fluorescence microscope (Nikon TE 2000-U, Nikon Instruments Inc.). Neuron induction experiment**:** PC-12 cells with a density of 1000 cells / well were seeded on a climbing slice with a diameter of 14 mm. After induction with NGF (50 ng / ml) for three days, the cells were fixed for 30 min and treated with 0.5% Triton-100 for 30 min. PBS was washed three times (all subsequent operations should be avoided light). FITC-phalloidin was diluted at a ratio of 1:200 and incubated for 1 h. Subsequently, the sample was washed three times with PBS before DAPI 1:200 staining for 10 min., and photos were taken using a laser confocal microscope (Zeiss LSM900). The FITC-phalloidin and 4'6 diamidino-2-phenvlindole (DAPI) were purchased from Beijing Solarbio Science & Technology Co., Ltd. **Total RNA extraction and real-time fluorescence quantitative qPCR:** Total RNA was extracted using the Trizol method (TSP401, Tsingke Biotechnology Co., Ltd). RT SuperMix (K1074, APExBIO, Houston, USA) was used to reverse transcribe mRNA into cDNA. Subsequently, qPCR was performed using 2 × SYBR Green Master Mix (with ROX) (Shandong Sparkjade Biotech-nology Co., Ltd. (China)) on the QuantStudio 7 Flex system (Applied Biosystems, USA). The primer sequences used are shown in Table S1.

2.5. In vivo studies

Subcutaneous implant model: SD rats weighing 220 ± 10 g were selected. The animal study was reviewed and approved by the Biomedical Research Ethics Committee of Central South University. After a 3-day adaptation period, they were anesthetized with intraperitoneal injection of 3% pentobarbital sodium. A 1 cm longitudinal incision was made on the dorsal side, and an 8 mm diameter membrane was placed and flattened. After two weeks, skin tissue was obtained for histological staining.**Bone Defect Model:** SD rats weighing 220 ± 10 g were selected. After a 3-day adaptation period, they were anesthetized with intraperitoneal injection of 3% pentobarbital sodium. A 1 cm longitudinal incision was made at the central top of the skull. The skin was blunt separated, and the periosteum was removed. Using a hand-held drill with a 4.5 mm diameter bit, a hole was drilled on each side of the skull, and the bone fragments were peeled off. Then, a 6 mm diameter membrane was placed in each defect, the skin was sutured. After 6 weeks, the skull was obtained for micro-CT scanning to reconstruct the bone. The bone volume fraction (BV/TV) at the defect site was calculated, and after 21 days of decalcification, tissue sections were stained. The Double label multiple immunofluorescence kit was purchased from AiFangBiological (AFIHC023).

2.6. Statistical method

All experiments were performed at least three times. Data were analyzed using GraphPad Prism 9 software. One-way ANOVA was used to analyze the differences between normal distribution values of three or more experimental groups. $P < 0.05$ indicates a statistically significant difference.

3. Results and discussion

3.1. Material morphology and element distribution

First, we drew a schematic diagram of the material preparation process that roughly describes the preparation process of the Ta/WH nanoparticle-loaded bio-functionalized membrane. TaNPs and WH NPs are uniformly distributed in the design (Fig. 1A). Subsequently, images taken at 1000 × and 5000 × magnification by scanning electron microscopy (SEM) further show that the morphology of the spinning changes with the addition of TaNPs and WH NPs. The red and blue arrows point to TaNPs and WH NPs, respectively, confirming their uniform distribution (Fig. 1B). EDS spectrum analysis (Fig. 1C-F) shows that there is tantalum element in PCL/Ta, and tantalum, magnesium, calcium and other elements in WH, indicating that the distribution of each element conforms to the material design, and the distribution trend is consistent with SEM images.

3.2. Material performance analysis

To confirm the successful preparation of the material, we conducted an XRD experiment. The XRD pattern in Fig. 2A mainly shows the characteristic diffraction peaks of PCL, Ta and WH. The main diffraction peaks of PCL are at 21.42° and 23.84 ℃, those of Ta are at 38.24°, and those of WH are at 31.23°. The results proves that the membrane spinning with Ta and WH nanoparticles added is in conformity and no other impurities are produced during the preparation process. The water contact angle is an important parameter for measuring the hydrophilicity or hydrophobicity of a biomaterial. The larger the water contact angle, the more hydrophobic the material surface is; conversely, the smaller the water contact angle, the more hydrophilic it is. The water contact angles of each spun film in Fig. 2B are 129 ± 1.33°, 128.67 ± 1.89°, and 128.76 ± 1.44°, respectively, indicating that its hydrophilicity did not increase significantly after adding TaNPs and did not change after adding WH NPs. It was found in Fig. 2C that its tensile properties decreased to some extent after adding NPs, possibly due to excessive WH causing stress concentration inside the composite material and thus reducing it[32]. Studies have shown that local ion concentration may affect BMSCs osteogenic differentiation[34]. We speculate that Mg^{2+} rich in WH has an important effect on neurovascularization into bone. Therefore, we explored its relationship with neurovascularization into bone by testing Mg^{2+} release trend in Fig. 2D, which shows that PCL/Ta/WH membrane can achieve a sustained release for up to two weeks, reaching 80% of the release amount on the third day and then decreasing until reaching equilibrium release amount on the tenth day, proving that it can have an effect on osteogenesis *in vivo*, and the cumulative release amounts for the WH at 14days were 87.5 μM, which the physiologically acceptable range.

3.3. Effect on angiogenesis

Cell compatibility refers to the interaction between a material and cells in a biological organism, which can maintain the normal function and structure of cells without causing damage or death. Cell

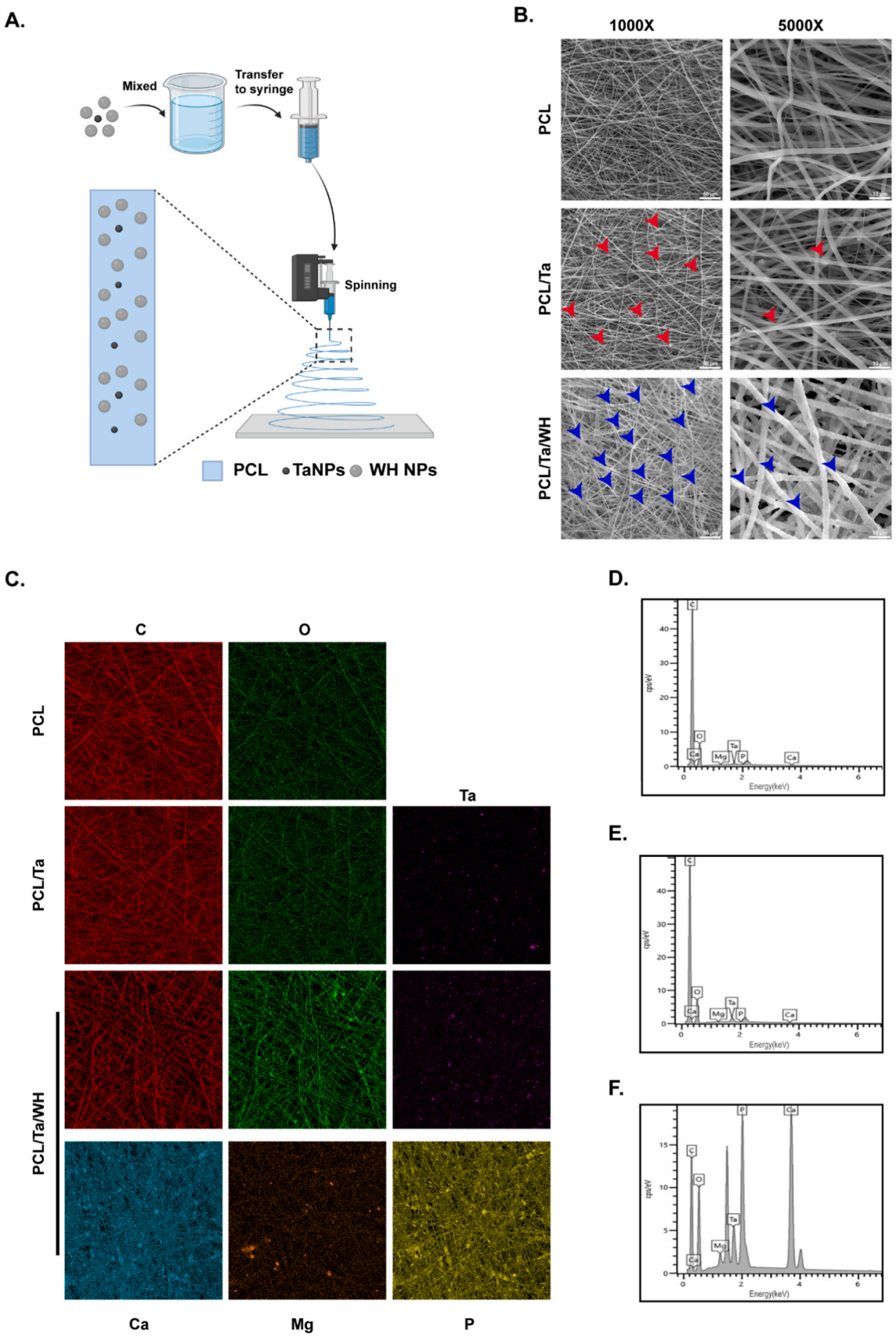

Fig. 1. (A) Schematic diagram illustrating the process of material preparation; (B) Scanning electron microscopy (SEM) images depicting the surface morphology of the material, with red arrows indicating Ta NPs and blue arrows indicating WH NPs; (C) Energy dispersive X-ray spectroscopy (EDS) analysis revealing the elemental composition of the material; (D-F) display EDS analysis spectra for PCL, PCL/Ta, and PCL/Ta/WH nanofiber membranes, respectively.

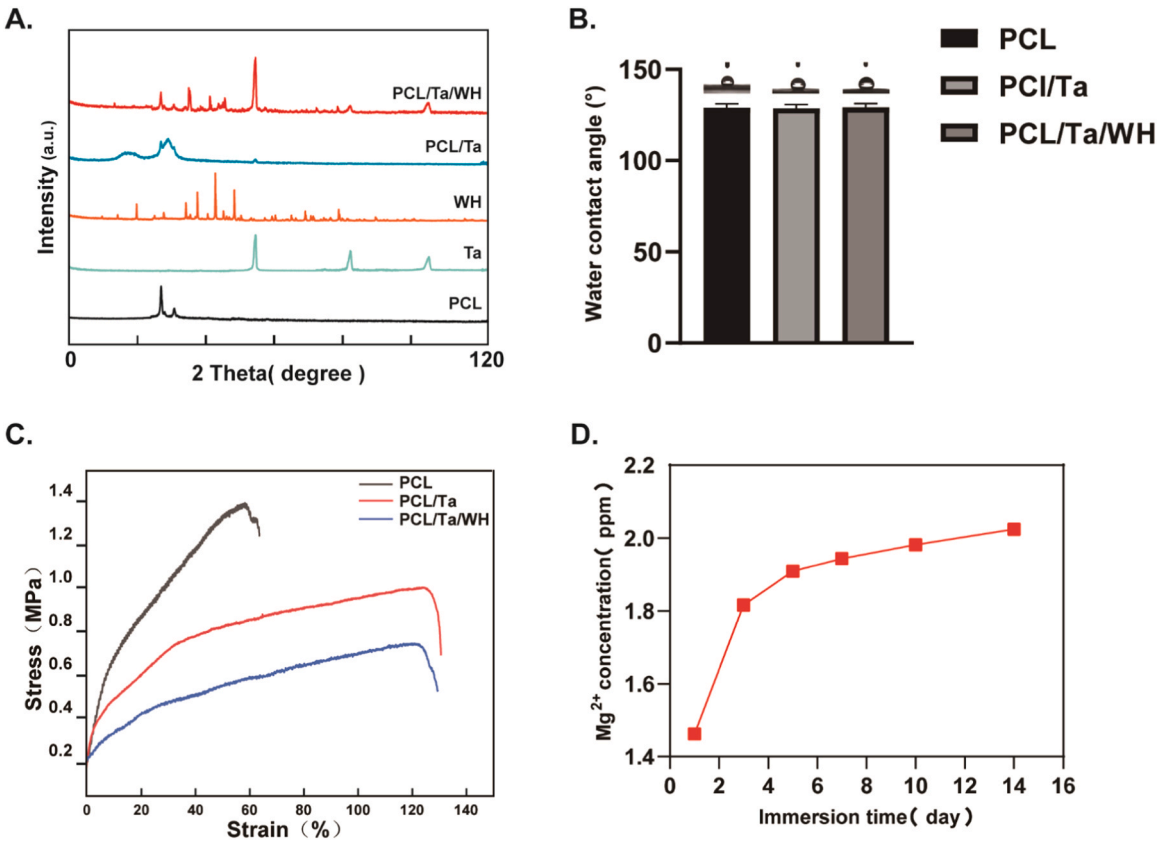

Fig. 2. (A) The crystal structure of the material is revealed by X-ray diffraction (XRD) pattern; (B) Water contact angles are indicated by each nanofiber film; (C) Stress-strain curves of different nanofiber films are presented; (D) Mg^{2+} release curve from PCL/Ta/WH nanofibrous membranes.

compatibility is an important indicator for evaluating the application of biomaterials *in vivo* and is also the core content of biomaterial research. The quality of cell compatibility depends on the physical, chemical and biological characteristics of the material, as well as the type, state and environment of the cells. Through the study of cell compatibility, theoretical basis and experimental data can be provided for the design, modification and application of biomaterials. In order to prove the cell compatibility of PCL/Ta/WH with RAECs, we first conducted a CCK8 proliferation experiment. The proliferation effect of RAECs on each group of membranes containing NPs was not significantly affected (Fig. 3A). At the same time, we also conducted live/dead tests to prove whether it has cell toxicity to RAECs. As shown in Fig. 3B, the results showed that PCL/Ta/WH membrane had no significant cell toxicity to RAECs. In bone defect repair, vascularization is an essential part because it can provide nutrition and oxygen for osteoblasts, thereby promoting bone tissue formation and reconstruction[35,36]. Our previous research results have found that Ta nanoparticles can stimulate endothelial cell proliferation and migration by regulating the immune microenvironment and increasing the number of M2 macrophages and vascular endothelial growth factor secretion[30]. WH may promote endothelial cell differentiation and tube formation by activating Wnt/β-catenin signaling pathway[37]. In order to explore the effect of adding WH and Ta on angiogenesis, we conducted a tube formation experiment using RAECs as a model. Fig. 3C shows the formation of a microvascular network under a microscope, indicating that PCL/Ta group has a promoting effect on angiogenesis, and PCL/Ta/WH membrane has a stronger promoting effect on angiogenesis than membranes containing Ta NPs, with significant differences. In order to specifically demonstrate the difference in tube differentiation, we also performed statistical analysis on the vascular network to compare differences in Tot. branching length, Nb nodes, Nb meshes, Nb master junctions among groups. The results showed that PCL/Ta membrane and PCL/Ta/WH membrane induced more small vascular networks in early stage (Fig. 3D-G) and had better angiogenic properties.

3.4. Promote neurogenesis ability

Neuralized bone regeneration is currently a research focus. Within cortical bone, nerve fibers predominantly follow the course of blood vessels, traverse both periosteal and endosteal layers, and penetrate into the osseous matrix[38]. In cancellous bone, nerve fibers form a complex network that runs along the bone trabeculae and blood vessels. Within the bone marrow, nerve fibers are primarily concentrated around blood vessels, creating a dense neural plexus[39]. These nerve fibers closely interact with hematopoietic stem cells, osteoblasts, and osteoclasts to potentially facilitate bone repair through neural-bone regulation or neural-vascularization[40]. RSCs and PC12 cells were utilized as models to investigate the effects of Ta and WH on nerve regeneration. CCK8 proliferation assay was employed to validate the proliferative effect of RSCs on PCL, PCL/Ta, and PCL/Ta/WH membranes at days 1 and 3. Results indicated that NPs-containing membrane had no significant impact on RSCs proliferation (Fig. 4A). We conducted both *in vitro* and *in vivo* experiments to investigate the potential toxicity of PCL/Ta and PCL/Ta/WH membranes towards RSCs. The results demonstrated that neither membrane exhibited any cytotoxicity towards RSCs (Fig. 4B). Fig. 4C demonstrates the robust ability of PCL/Ta/WH membrane to induce migration of RSCs, resulting in spindle-filament morphology. Semi-quantitative analysis reveals that the PCL/Ta/WH group exhibits significantly higher migration effect on RSCs compared to the PCL group (Fig. 4D). Mg^{2+} serves as a crucial neurotransmitter that modulates the excitability and signal transduction of nerve cells. Recent research indicates its potential in promoting bone regeneration through neural-bone regulation or neurovascularization[41]. Fig. 4E-F demonstrates that the addition of WH leads to an increase in both the number of

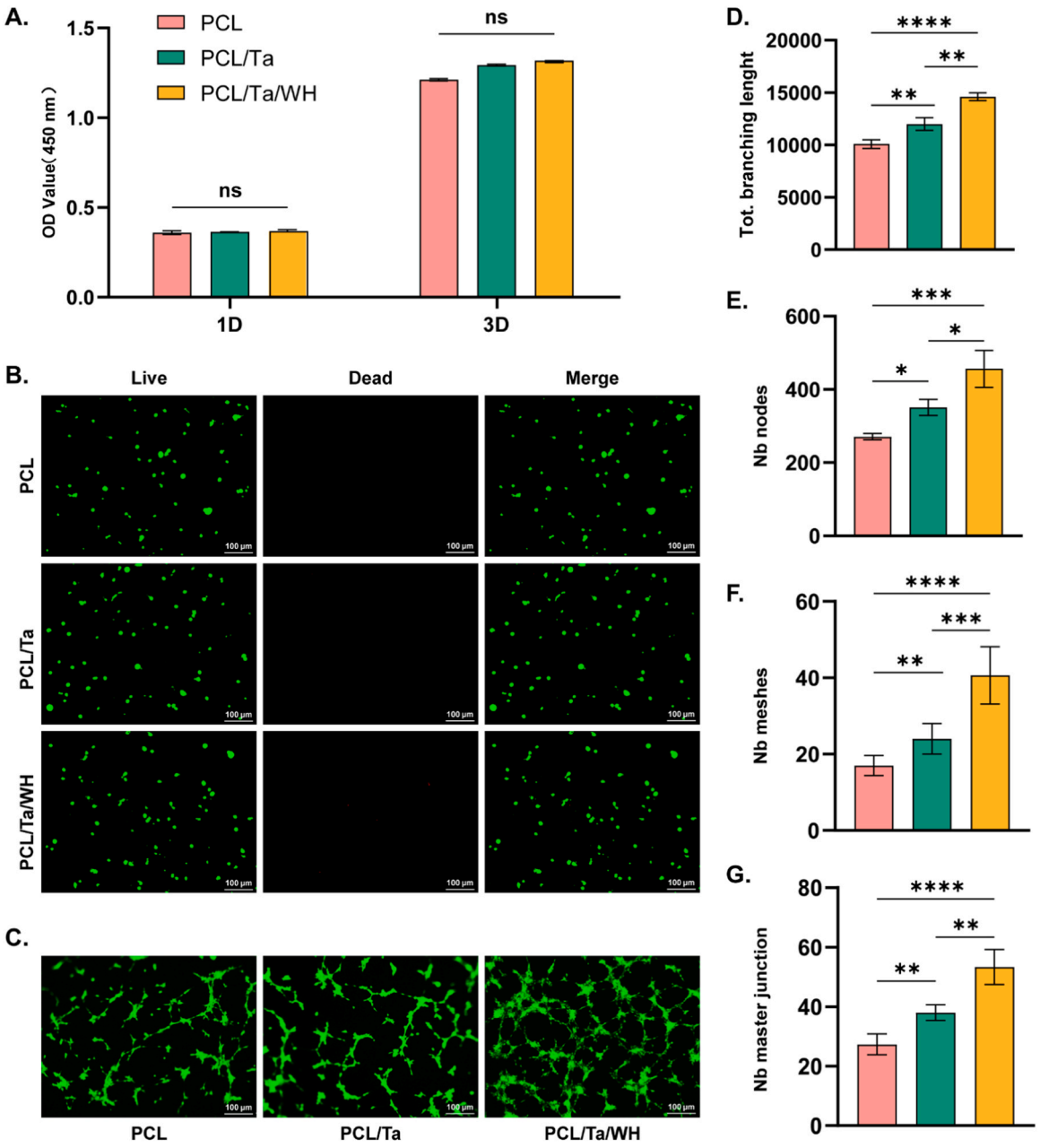

Fig. 3. The assessment of cytocompatibility and tube differentiation of rat aortic endothelial cells (RAECs) on various nanofiber membranes.(A)The CCK8 assay was conducted to evaluate cell growth after 1 and 3 days of culture;(B) After one day of toxicity experiment on nanofiber membrane, RAECs were stained with Calcein-AM for live cells and propidium iodide (PI) for dead cells;(C)The experimental results were obtained by using Calcein-AM staining to observe the formation of tube-like structures in RAECs after 8 h of intervention with various nanofiber membrane extracts;(D-G) Using ImageJ for semi-quantitative analysis of tubu formation experiments, including Tot. branching length, Nb nodes, Nb meshes and Nb master junctions.

branches and length of axons, while significantly enhancing neuronalization in PC-12 cells. Semi-quantitative analysis *via* RT-qPCR revealed that PCL/Ta/WH nanofiber membranes significantly up-regulated the expression levels of neuralization-related genes (BDNF, NGF, S100) (Fig. 4G-I). These results suggest that WH can effectively promote functionalization of vascular endothelium and nerve cells, which is consistent with previous literature[42]. In summary, it is speculated that the sustained release of Mg^{2+} from WH may facilitate local nerve vascularization and accelerate bone defect repair.

3.5. Effect on osteogenesis in vitro

The assessment of bone repair materials' performance hinges on their ability to promote bone formation, which is the most fundamental characteristic of biomaterials. To demonstrate PCL/Ta/WH membranes' *in vitro* osteoinductive potential, BMSCs were seeded onto these membranes and subjected to osteogenic induction. Alkaline phosphatase (ALP) activity, Sirius red, alizarin red, and gene expression were assessed. As depicted in Fig. 5A-B, ALP staining revealed weaker activity in the PCL group compared to the PCL/Ta group. Notably, the PCL/Ta/WH group exhibited the highest level of ALP activity. As depicted in Fig. 5C-D, Sirius staining was conducted on the surface collagen of each group at 7 and 14 days. The PCL/Ta/WH group exhibited the highest staining intensity, while the PCL group displayed the lowest staining intensity. The quantitative results obtained after dye elution were consistent with the aforementioned staining outcomes. As depicted in

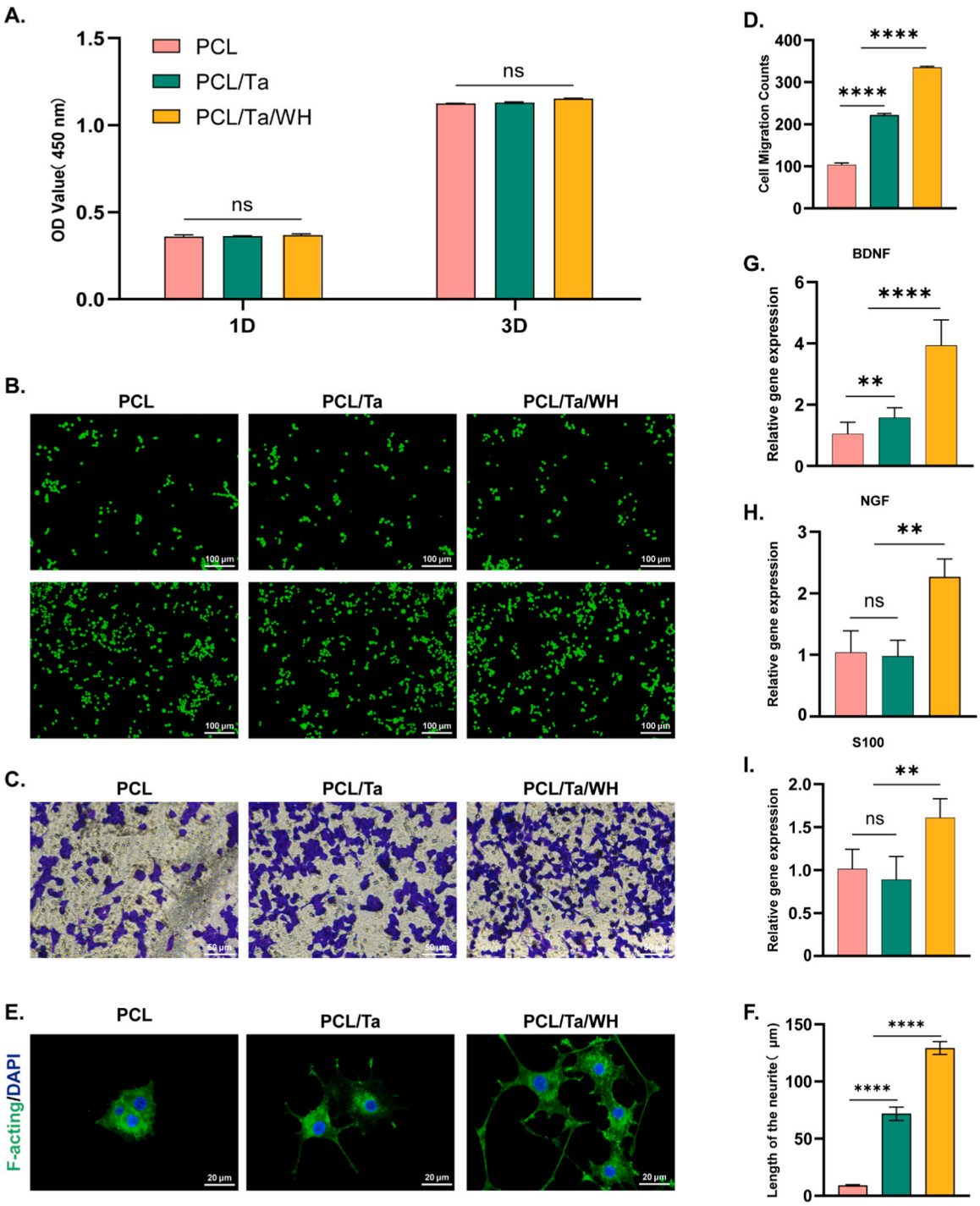

Fig. 4. The cytocompatibility of each nanofiber membrane with RSCs and its impact on the neural differentiation of PC-12 cells. (A) The CCK8 proliferation assay results for RSCs cultured on nanofiber membranes were obtained after 1 and 3 days in each group ; (B) After 1 and 3 days of toxicity experiments on nanofiber membranes, RSCs were stained with Calcein-AM for live cells and PI for dead cells ; The migration test results (C) and counting analysis (D) of RSCs induced by each nanofiber membrane *via* Transwell assay ; (E-F) The PC-12 cytoskeleton was stained on each nanofiber membrane, and analysis neurite length ; (G-I) RT-qPCR was used to detect neural-related gene expression (BDNF, NGF, S100) in each group after 5 days of RSCs growth on the nanofiber membranes.

Fig. 5E-F, the surface calcium nodules of each group were subjected to ARS staining at 14 and 21 days. The PCL/Ta/WH group exhibited the most intense staining, while the PCL group displayed the weakest staining. The quantitative results obtained after dye elution were consistent with the aforementioned observations, and inter-group differences were statistically significant. To assess the expression levels of genes related to osteogenesis, we conducted RT-qPCR experiments to extract total RNA from BMSCs cultured on each membrane for 5 days and semi-quantitatively analyzed the expression of osteogenesis-related genes (OCN, BMP, Runx2), which confirmed that PCL/Ta/WH membranes could enhance osteogenesis at the molecular level (Fig. 5G-I). Previous research has demonstrated that the synergistic interplay among nanoparticles within the material system exerts a beneficial influence on both cell proliferation and osteogenic differentiation[43]. The role of Ta and WH, as well as their potential mechanism, were deliberated upon, leading to the speculation that Ta and WH may act synergistically in

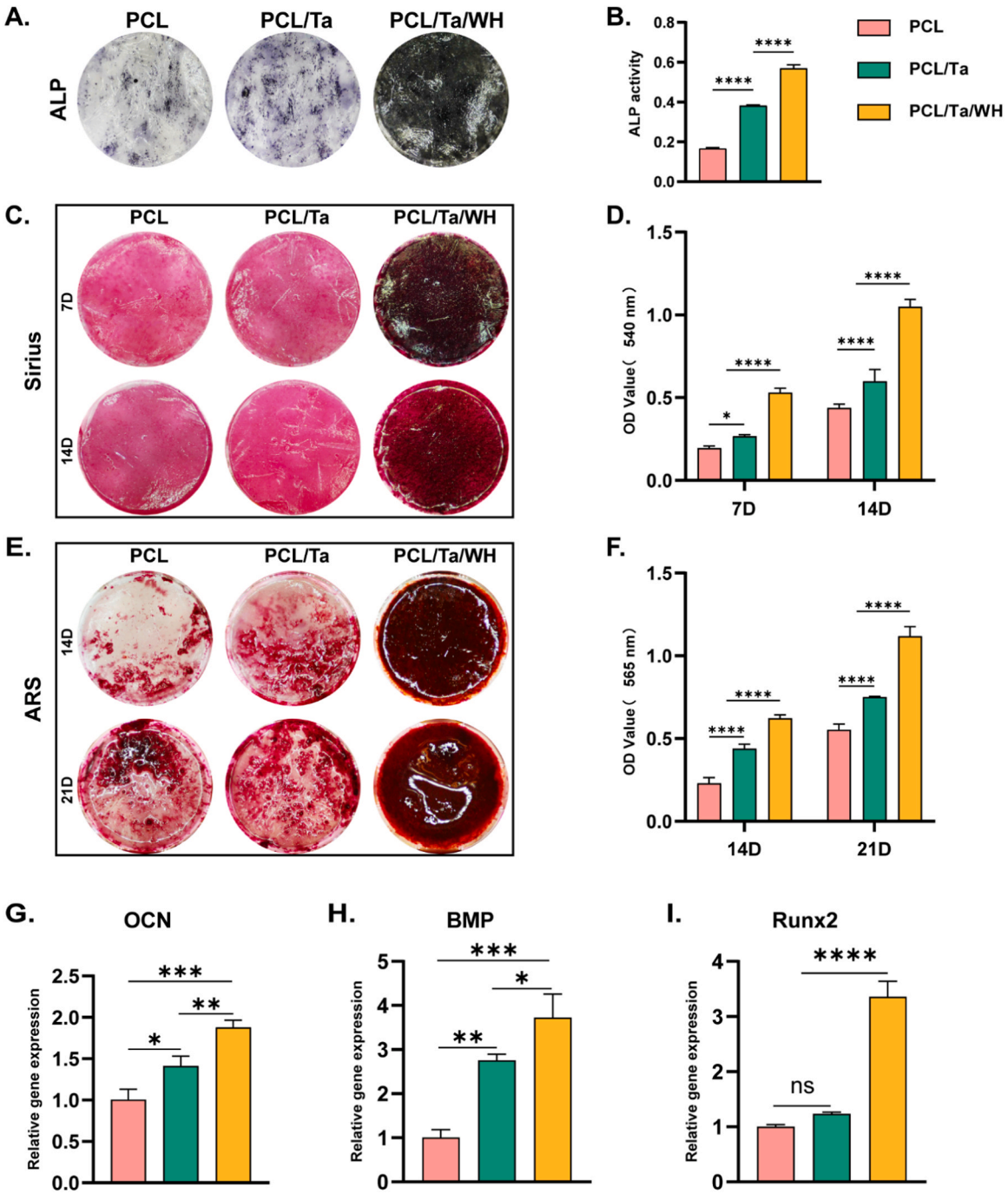

Fig. 5. The results of *in vitro* osteogenesis experiment.(A-B)ALP staining was utilized for the semi-quantitative analysis of ALP expression on each nanofiber membrane of BMSCs 7 days after osteogenic induction;(C-D)Sirius staining was employed to visualize the collagen content, and semi-quantitative analysis was conducted on each nanofiber membrane of BMSCs after 7 and 14 days of osteogenic induction;(E-F)Alizarin red staining was utilized to observe the calcium nodule content on each nanofiber membrane following 14 and 21 days of osteogenic induction;(G-I) After 7 days of inducing osteogenesis, RT-qPCR was used to evaluate the expression of key genes related to bone formation (OCN, BMP, Runx2) in all experimental groups.

promoting bone regeneration.

3.6. Ability to induce angiogenesis in vivo

To investigate the *in vivo* impact of PCL/Ta/WH membranes on angiogenesis, 1-week and 2-week skin tissues were subjected to H&E and Masson staining. In Fig. 6A-B, the red arrow indicates neovascularization, and the PCL/Ta/WH group significantly promotes angiogenesis. Fig. 6C-D demonstrates that while promoting angiogenesis, the muscle fibers and collagen fibers of the PCL/Ta/WH group are also significantly greater than those of the other two groups, indicating that the reparative effect of the PCL/Ta/WH group on surrounding skin is also superior. Immunofluorescence staining was conducted on the skin tissue samples from each group (Fig. 6E). The PCL/Ta/WH group exhibited the highest expression of CD31, as well as increased α-SMA expression. Semi-quantitative analysis of CD31 and α-SMA fluorescence intensity was performed (Fig. 6F-G), and a consistent trend was observed.

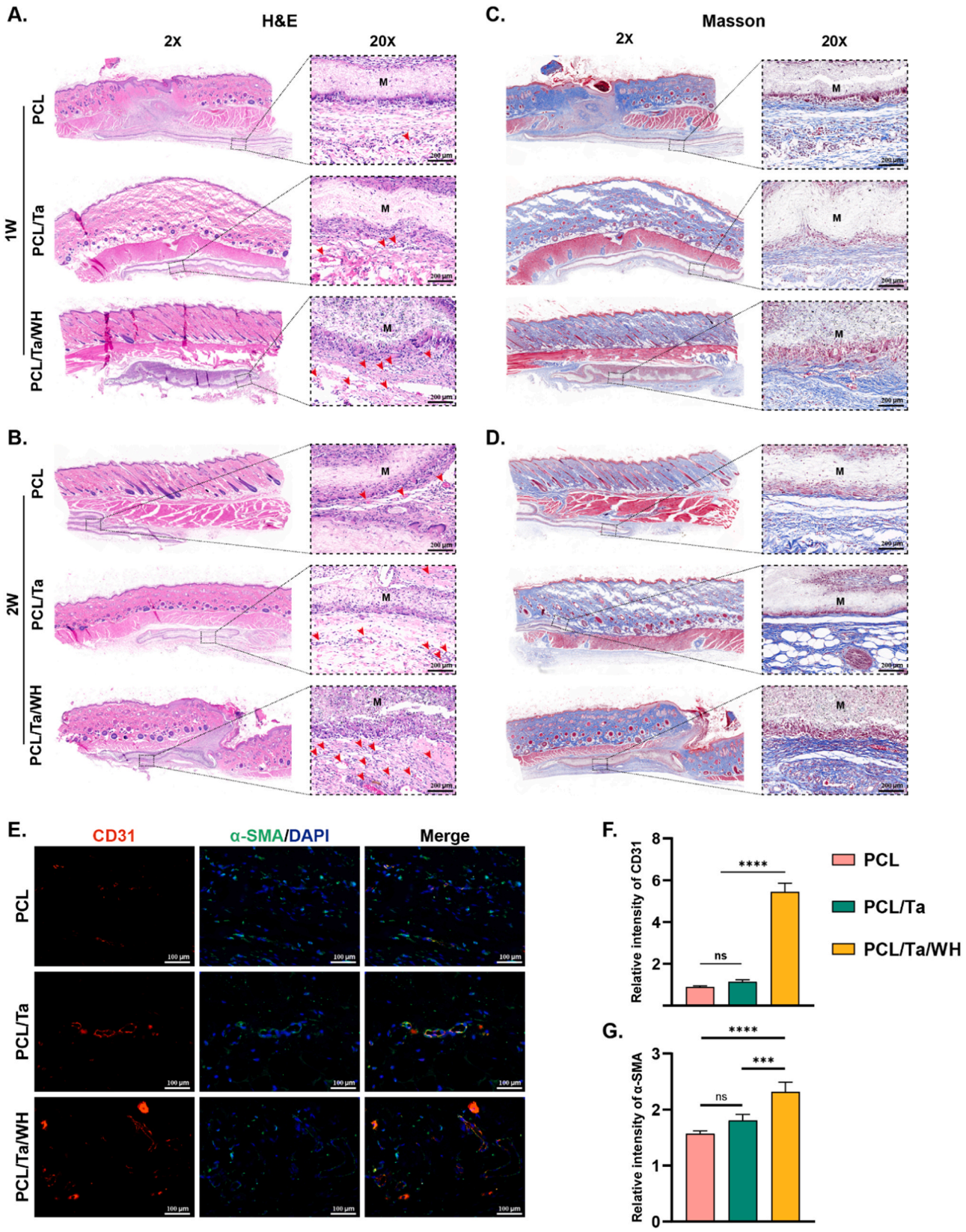

Fig. 6. Immunological analysis of subcutaneous tissue. Low (2-fold) and high (20-fold) (A-B) H&E staining and (C-D) Masson trichrome staining were performed at weeks 1 and 2(the red arrow indicates neovascularization while M denotes the nanofiber membrane.); (E-G) Representative images of α-SMA (green) and CD31 (red) immunofluorescence staining, along with CD31 α-SMA and fluorescence intensity in each field. DAPI-stained nuclei.

3.7. Functional membrane for the repair of cranial defects

To validate our proposed method of inducing bone regeneration, we introduced a critical bone defect model in the rat skull and removed the pericranial periosteum, as depicted in Fig. 7A. The process of bone formation was evaluated macroscopically and microscopically using Micro-CT and histological analysis at 6 weeks post-surgery, respectively. As depicted in Fig. 7B of the 3D reconstruction, the PCL/Ta/WH group exhibited a significant reparative effect, while the PCL/Ta group also outperformed the WH group. This was further confirmed by analyzing total bone volume (BV) and bone volume fraction (BV/TV) (Fig. 7C-D). The BV analysis revealed that the volume of PCL/Ta/WH group (51.09 ± 4.83%) was twice as high as that of the PCL group (28.35 ± 8.66%). BV/TV analysis revealed that the PCL/Ta/WH group exhibited a significantly higher value (51.09 ± 4.83%) compared to the PCL group (28.35 ± 8.66%), indicating a two-fold increase in bone volume fraction. Additionally, the PCL/Ta group also showed a slightly elevated BV/TV ratio (35.92 ± 3.58%) relative to the PCL group (28.35 ± 8.66%). These findings are consistent with overall assessments and were further confirmed by histological examination of defect areas. We utilized H&E and Masson staining techniques to differentiate between newly formed bone and host bone within the 4.5 mm defect area. Subsequently, we scrutinized the Masson-stained images at a higher magnification to assess both central and edge regions of the defect site. Our findings revealed that the PCL/Ta/WH group exhibited superior bone tissue formation and regeneration compared to other groups (Fig. 7E).

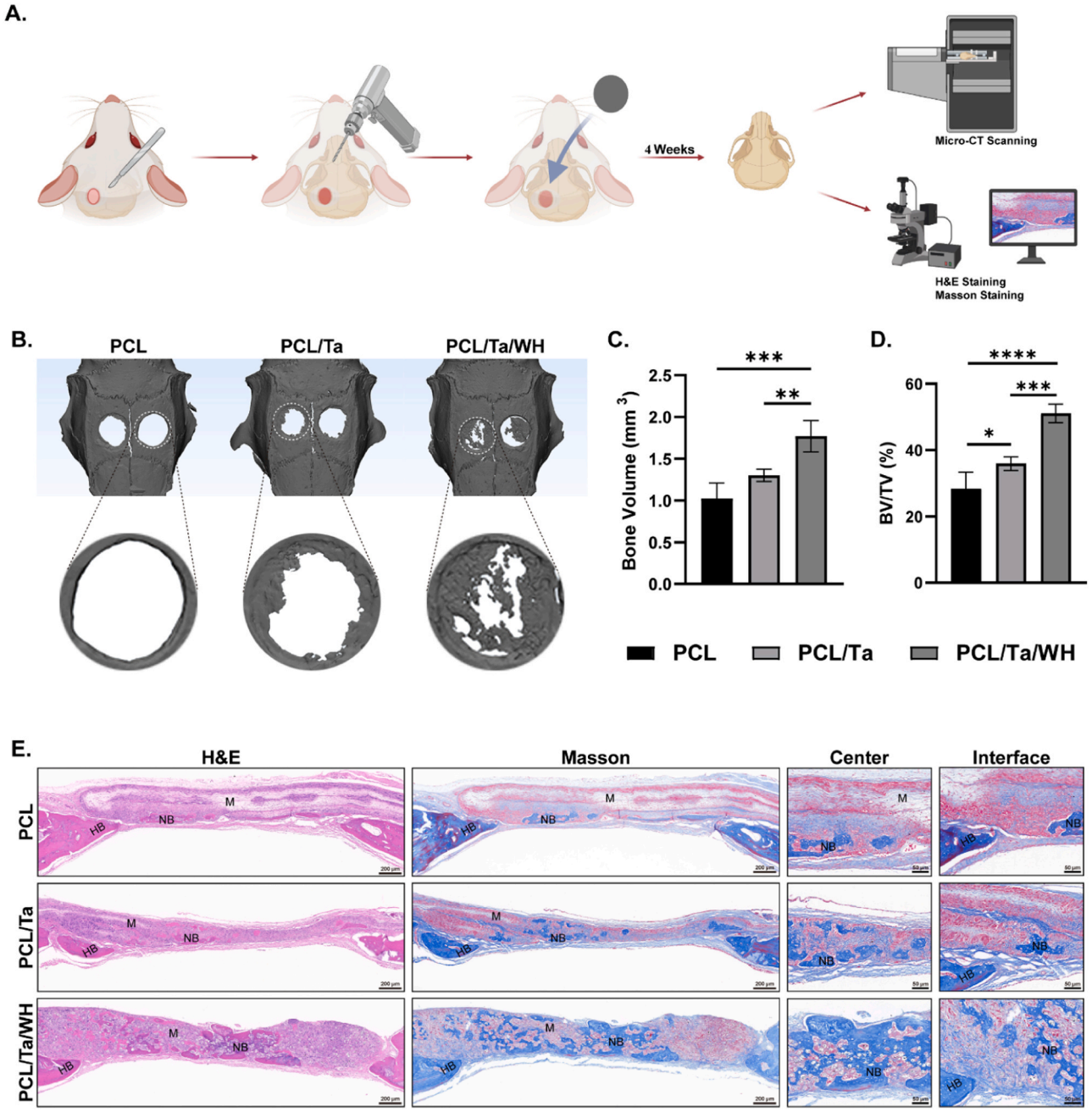

Fig. 7. Comprehensive Evaluation of osteogenic ability in vivo.(A) A diagram showing the steps to create and assess a bone defect model;(B) 3D reconstruction of the defect area; Statistical analysis of (C) Total bone volume(BV) and (D) Bone volume fraction(BV/TV);(E) Low (4X) and high (15X) H&E staining and Masson trichrome staining were performed at week 6. (M, the nanofibrous membrane; NB, the new bone, and HB, the host bone).

3.8. Neurovascular coupling enhances bone regeneration

To confirm the osteogenic promotion effect of PCL/Ta/WH membrane through neurovascular coupling, we performed CD31/β3-Tubulin double immunofluorescence staining and Perionstin/OCN double immunofluorescence staining on the 6-week postoperative skull. The distribution of neurovascular-related factors (CD31 and β3-Tublin) within the bone defect area was observed. Compared to the PCL group, both PCL/Ta group and PCL/Ta/WH group showed enhanced expression, with a more significant effect observed in the latter (Fig. 8A). $CD31^+$ area percentage analysis revealed significantly higher values for PCL/Ta/WH (3.13 ± 0.055%) compared to PCL group (0.26 ± 0.017%), and slightly higher values for PCL/Ta group (0.53 ± 0.072%) compared to PCL group (0.26 ± 0.017%) (Fig. 8B). Similarly, β3-$Tubulin^+$ area percentage analysis showed significantly higher values for PCL/Ta/WH (4.18 ± 0.36%) compared to PCL group (0.12 ± 0.008%), and slightly higher values for PCL/Ta group (0.268 ± 001%) compared to PCL group (0.12 ± 0.008%) (Fig. 8C). The distribution of osteogenic factors (periostin and OCN) in the bone defect area was observed. Compared to the PCL group, expression levels were enhanced in both the PCL/Ta and PCL/Ta/WH groups, with periostin primarily expressed around the nanofiber membrane (Fig. 8D). The analysis of the $Perionstin^+$ area percentage revealed that the PCL/Ta/WH group exhibited significantly higher values (3.82 ± 0.216%) compared to both the PCL (0.24 ± 0.044%) and PCL/Ta groups (0.87 ± 0.174%). Similarly, the OCN^+ area percentage analysis demonstrated a significant increase in the PCL/Ta/WH group (5.72 ± 0.187%), as compared to both the PCL (3.37 ± 0.284%) and PCL/Ta groups (4.11 ± 0.229%) (Fig. 8E and F). The aforementioned findings suggest that PCL/Ta/WH nanofibrous membranes promote the formation of a high-density neurovascular network at the bone defect site, and exhibit excellent osteoinductive potential for achieving high-quality bone regeneration.

4. Conclusion

In summary, we have successfully fabricated a cytocompatible osteoinductive membrane that promotes bone regeneration through neurovascular coupling and creates a favorable microenvironment for bone formation during the repair of critical bone defect. Based on the degradable properties of PCL and the scaffold's role, doped Ta and WH nanoparticles can persist for an extended period to establish a high-density neurovascular network microenvironment that achieves optimal osteoinductive regeneration effects and promotes high-quality bone defect repair. *In vitro* and *in vivo* studies have demonstrated that PCL/Ta/WH nanofibrous membranes possess robust osteogenic potential in BMSCs while also significantly impacting neurovascular repair. *In vivo* studies have confirmed the formation of a high-density neurovascular network surrounding PCL/Ta/WH nanofibrous membranes. The secretion of neurovascular factors greatly accelerates bone regeneration, shortens the natural healing process of bone formation, and achieves high-quality repair of bone defects.

CRediT authorship contribution statement

Kai Zhang: Conceptualization, Methodology, Validation, Formal analysis, Investigation, Data curation, Writing – original draft, Writing – review & editing, Visualization. **Hongkun Hu**: Validation, Formal analysis, Investigation, Writing–review & editing. **Yan Sun**: Conceptualization, Methodology, Writing – review & editing. **Jiangyu Nan**: Validation, Formal analysis, Investigation. **Wenbin Liu**: Methodology, Writing – review & editing. **Pengfei Lei**: Conceptualization, Writing – review & editing, Supervision, Project administration, Funding

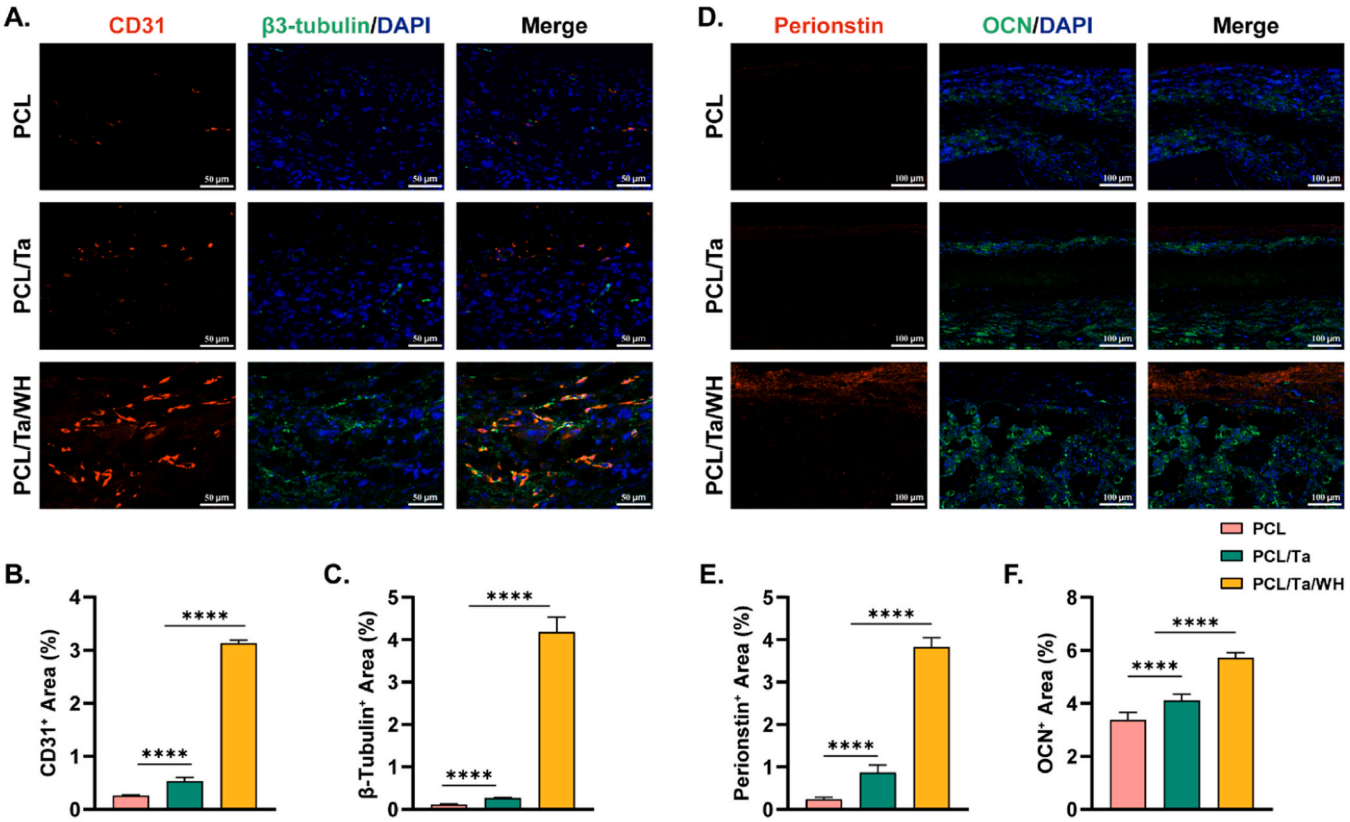

Fig. 8. Immunofluorescence staining analysis of CD31, β3-tubulin, Perionstin and OCN in bone defects. (A) Representative images of CD31 and β3-tubulin double staining and semi-quantitative analysis of (B) CD31 (red) and (C) β3-tubulin (green); (D)representative images of double staining for Perionstin and OCN, along with the semi-quantitative analysis results of (E) Perionstin (red) and (F) OCN (green), respectively; the nuclei were stained with DAPI (blue).

acquisition. **Yihe Hu**: Conceptualization, Formal analysis, Funding acquisition, Writing – review & editing.

Declaration of Competing Interest

The authors declare that they have no known competing financial interests or personal relationships that could have appeared to influence the work reported in this paper.

Data Availability

The data that has been used is confidential.

Acknowledgements

This study was supported by the Natural Science Foundation of China (grant nos. 82272452), Key Project of Research and Development Plan of Hunan Province (grant nos. 2020SK2008,2021GK2012), Hunan Provincial Natural Science Foundation (grant nos. 2022JJ40754, 2021JJ40929), and Fundamental Research Funds for Central Universities of the Central South University.

Appendix A. Supporting information

Supplementary data associated with this article can be found in the online version at doi:10.1016/j.colsurfb.2023.113506.

References

[1] P. Baldwin, D.J. Li, D.A. Auston, H.S. Mir, R.S. Yoon, K.J. Koval, Autograft, allograft, and bone graft substitutes: clinical evidence and indications for use in the setting of orthopaedic trauma surgery, J. Orthop. Trauma 33 (4) (2019) 203–213.
[2] J.A. Ankrum, J.F. Ong, J.M. Karp, Mesenchymal stem cells: immune evasive, not immune privileged, Nat. Biotechnol. 32 (3) (2014) 252–260.
[3] Y. Shiba, T. Gomibuchi, T. Seto, Y. Wada, H. Ichimura, Y. Tanaka, T. Ogasawara, K. Okada, N. Shiba, K. Sakamoto, D. Ido, T. Shiina, M. Ohkura, J. Nakai, N. Uno, Y. Kazuki, M. Oshimura, I. Minami, U. Ikeda, Allogeneic transplantation of iPS cell-derived cardiomyocytes regenerates primate hearts, Nature 538 (7625) (2016) 388.
[4] L.G. Cui, J. Zhang, J. Zou, X.R. Yang, H. Guo, H.Y. Tian, P.B. Zhang, Y. Wang, N. Zhang, X.L. Zhuang, Z.M. Li, J.X. Ding, X.S. Chen, Electroactive composite scaffold with locally expressed osteoinductive factor for synergistic bone repair upon electrical stimulation, Biomaterials 230 (2020).
[5] Y. Lu, A.A. Aimetti, R. Langer, Z. Gu, Bioresponsive materials, Nat. Rev. Mater. 2 (1) (2017).
[6] I. Matai, G. Kaur, A. Seyedsalehi, A. McClinton, C.T. Laurencin, Progress in 3D bioprinting technology for tissue/organ regenerative engineering, Biomaterials 226 (2020).
[7] M. Janmohammadi, Z. Nazemi, A.O.M. Salehi, A. Seyfoori, J.V. John, M. S. Nourbakhsh, M. Akbari, Cellulose-based composite scaffolds for bone tissue engineering and localized drug delivery, Bioact. Mater. 20 (2023) 137–163.
[8] Z. Fu, Y. Zhuang, J. Cui, R. Sheng, H. Tomás, J. Rodrigues, B. Zhao, X. Wang, K. Lin, Development and challenges of cells- and materials-based tooth regeneration, Eng. Regen. 3 (2) (2022) 163–181.
[9] Y. Zhu, B. Kong, R. Liu, Y. Zhao, Developing biomedical engineering technologies for reproductive medicine, Smart Med. 1 (1) (2022), e20220006.
[10] C.Q. Zhao, P.C. Zhang, J.J. Zhou, S.H. Qi, Y. Yamauchi, R.R. Shi, R.C. Fang, Y. Ishida, S.T. Wang, A.P. Tomsia, L. Jiang, M.J. Liu, Layered nanocomposites by shear-flow-induced alignment of nanosheets, Nature 580 (7802) (2020) 210 (+).
[11] Y. Gao, Q. Ma, Bacterial infection microenvironment-responsive porous microspheres by microfluidics for promoting anti-infective therapy, Smart Med. 1 (1) (2022), e20220012.
[12] W. Liu, L. Liang, B. Liu, D. Zhao, Y. Tian, Q. Huang, H. Wu, The response of macrophages and their osteogenic potential modulated by micro/nano-structured Ti surfaces, Colloids Surf. B Biointerfaces 205 (2021), 111848.
[13] X.F. Wang, B. Ding, B.Y. Li, Biomimetic electrospun nanofibrous structures for tissue engineering, Mater. Today 16 (6) (2013) 229–241.
[14] L. Wu, Y. Gu, L.L. Liu, J.C. Tang, J.N. Mao, K. Xi, Z.R. Jiang, Y.D. Zhou, Y. Xu, L. F. Deng, L. Chen, W.G. Cui, Hierarchical micro/nanofibrous membranes of sustained releasing VEGF for periosteal regeneration, Biomaterials 227 (2020).
[15] H.X. Shen, J.Z. Liu, X.Q. Yan, H.N. Yang, S.Q. Hu, X.L. Yan, T. Xu, A.J. El Haj, Y. Yang, L.X. Lü, Hydrostatic pressure stimulates the osteogenesis and angiogenesis of MSCs/HUVECs co-culture on porous PLGA scaffolds, Colloids Surf. B Biointerfaces 213 (2022), 112419.
[16] T. Carvalho, N.Z. Ezazi, A. Correia, C. Vilela, H.A. Santos, C.S.R. Freire, Gelatin-lysozyme nanofibrils electrospun patches with improved mechanical, antioxidant and bioresorbability properties for myocardial regeneration applications, Adv. Funct. Mater. 32 (21) (2022).
[17] X. Chen, S.Y. Han, W.H. Wu, Z.H. Wu, Y. Yuan, J. Wu, C.S. Liu, Harnessing 4D printing bioscaffolds for advanced orthopedics, Small 18 (36) (2022).
[18] C.S. Lee, H.S. Hwang, S. Kim, J.B. Fan, T. Aghaloo, M. Lee, Inspired by nature: facile design of nanoclay-organic hydrogel bone sealant with multifunctional properties for robust bone regeneration, Adv. Funct. Mater. 30 (43) (2020).
[19] W. Qiao, H.Z. Xie, J.H. Fang, J. Shen, W.T. Li, D.N. Shen, J. Wu, S.L. Wu, X.Y. Liu, Y.F. Zheng, K.M.C. Cheung, K.W.K. Yeung, Sequential activation of heterogeneous macrophage phenotypes is essential for biomaterials-induced bone regeneration, Biomaterials 276 (2021).
[20] Y. Peng, S. Wu, Y.S. Li, J.L. Crane, Type H blood vessels in bone modeling and remodeling, Theranostics 10 (1) (2020) 426–436.
[21] A.P. Kusumbe, S.K. Ramasamy, R.H. Adams, Coupling of angiogenesis and osteogenesis by a specific vessel subtype in bone, Nature 507 (7492) (2014) 323.
[22] L. Lü, A. Deegan, F. Musa, T. Xu, Y. Yang, The effects of biomimetically conjugated VEGF on osteogenesis and angiogenesis of MSCs (human and rat) and HUVECs co-culture models, Colloids Surf. B Biointerfaces 167 (2018) 550–559.
[23] Y.F. Zhang, J.K. Xu, Y.C. Ruan, M.K. Yu, M. O'Laughlin, H. Wise, D. Chen, L. Tian, D.F. Shi, J.L. Wang, S.H. Chen, J.Q. Feng, D.H.K. Chow, X.H. Xie, L.Z. Zheng, L. Huang, S. Huang, K. Leung, N. Lu, L. Zhao, H.F. Li, D.W. Zhao, X. Guo, K. M. Chan, F. Witte, H.C. Chan, Y.F. Zheng, L. Qin, Implant-derived magnesium induces local neuronal production of CGRP to improve bone-fracture healing in rats, Nat. Med. 22 (10) (2016) 1160–1169.
[24] Q. Qin, S. Lee, N. Patel, K. Walden, M. Gomez-Salazar, B. Levi, A.W. James, Neurovascular coupling in bone regeneration, Exp. Mol. Med. 54 (11) (2022) 1844–1849.
[25] F. Elefteriou, J.D. Ahn, S. Takeda, M. Starbuck, X.L. Yang, X.Y. Liu, H. Kondo, W. G. Richards, T.W. Bannon, M. Noda, K. Clement, C. Vaisse, G. Karsenty, Leptin regulation of bone resorption by the sympathetic nervous system and CART, Nature 434 (7032) (2005) 514–520.
[26] T. Worzfeld, S. Offermanns, Semaphorins and plexins as therapeutic targets, Nat. Rev. Drug Discov. 13 (8) (2014) 603–621.
[27] P.Z. Zhuang, Y. Yao, X.X. Su, Y.A. Zhao, K. Liu, X.P. Wu, H.L. Dai, Vascularization and neuralization of bioactive calcium magnesium phosphate/hydrogels for wound healing, Compos. Part B-Eng. 242 (2022).
[28] J. Zhang, B.Y. Zhang, Z.F. Zheng, Q.Y. Cai, J.C. Wang, Q. Shu, L.J. Wang, Tissue-engineered bone functionalized with MoS2 nanosheets for enhanced repair of critical-size bone defect in rats, Adv. Funct. Mater. 32 (13) (2022).
[29] Z. Luo, J. Che, L. Sun, L. Yang, Y. Zu, H. Wang, Y. Zhao, Microfluidic electrospray photo-crosslinkable κ-Carrageenan microparticles for wound healing, Eng. Regen. 2 (2021) 257–262.
[30] Y. Sun, T.Z. Liu, H.K. Hu, Z.X. Xiong, K. Zhang, X. He, W.B. Liu, P.F. Lei, Y.H. Hu, Differential effect of tantalum nanoparticles versus tantalum micron particles on immune regulation, Mater. Today Bio 16 (2022).
[31] Q. Li, W.B. Liu, W. Hou, X.P. Wu, W.Y. Wei, J.W. Liu, Y.H. Hu, H.L. Dai, Micropatterned photothermal double-layer periosteum with angiogenesis-neurogenesis coupling effect for bone regeneration, Mater. Today Bio 18 (2023).
[32] X.K. Zhang, W.B. Liu, J.W. Liu, Y.H. Hu, H.L. Dai, Poly-epsilon-caprolactone/Whitlockite Electrospun Bionic Membrane with an Osteogenic-Angiogenic Coupling Effect for Periosteal Regeneration, Acs Biomater. Sci. Eng. 7 (7) (2021) 3321–3331.
[33] G. Kazakova, T. Safronova, D. Golubchikov, O. Shevtsova, J.V. Rau, Resorbable Mg2+-containing phosphates for bone tissue repair, Materials 14 (17) (2021).
[34] Y.X. Lai, Y. Li, H.J. Cao, J. Long, X.L. Wang, L. Li, C.R. Li, Q.Y. Jia, B. Teng, T. T. Tang, J. Peng, D. Eglin, M. Alini, D.W. Grijpma, G. Richards, L. Qin, Osteogenic magnesium incorporated into PLGA/TCP porous scaffold by 3D printing for repairing challenging bone defect, Biomaterials 197 (2019) 207–219.
[35] A.P. Kusumbe, R.H. Adams, Osteoclast progenitors promote bone vascularization and osteogenesis, Nat. Med. 20 (11) (2014) 1238–1240.
[36] J. Zhou, H. Lin, T.L. Fang, X.L. Li, W.D. Dai, T. Uemura, J. Dong, The repair of large segmental bone defects in the rabbit with vascularized tissue engineered bone, Biomaterials 31 (6) (2010) 1171–1179.
[37] J.K. Lee, D. Kim, S.Y. Park, S.W. Baek, J.W. Jung, T.H. Kim, D.K. Han, Nitric oxide-releasing bioinspired scaffold for exquisite regeneration of osteoporotic bone via regulation of homeostasis, Adv. Sci. 10 (6) (2023).
[38] Z. Zhang, Z.C. Hao, C.H. Xian, Y.F. Fang, B. Cheng, J. Wu, J. Xia, Neuro-bone tissue engineering: multiple potential translational strategies between nerve and bone, Acta Biomater. 153 (2022) 1–12.
[39] Z.C. Hao, L. Ren, Z. Zhang, Z.W. Yang, S.J. Wu, G. Liu, B. Cheng, J. Wu, J. Xia, A multifunctional neuromodulation platform utilizing Schwann cell-derived exosomes orchestrates bone microenvironment via immunomodulation, angiogenesis and osteogenesis, Bioact. Mater. 23 (2023) 206–222.
[40] W.T. Li, W.Q. Miao, Y.H. Liu, T.C. Wang, Y.X. Zhang, W.H. Wang, D.Z. Lu, X. H. Zhou, X. Jiao, X.L. Jia, Y.X. Lin, Y.C. Li, H.T. He, Y.Q. Mao, Z.J. Ma, T. Li, J. W. Wang, Bioprinted constructs that mimic the ossification center microenvironment for targeted innervation in bone regeneration, Adv. Funct. Mater. 32 (9) (2022).
[41] Y. Xu, C. Xu, L. He, J.J. Zhou, T.W. Chen, L. Ouyang, X.D. Guo, Y.Z. Qu, Z.Q. Luo, D.Y. Duan, Stratified-structural hydrogel incorporated with magnesium-ion-

modified black phosphorus nanosheets for promoting neuro-vascularized bone regeneration, Bioact. Mater. 16 (2022) 271–284.

[42] Y.N. Zhao, H.L. Kang, X.P. Wu, P.Z. Zhuang, R. Tu, T. Goto, F. Li, H.L. Dai, Multifunctional Scaffold for Osteoporotic Pathophysiological Microenvironment Improvement and Vascularized Bone Defect Regeneration, Adv. Healthc. Mater. 12 (15) (2023).

[43] H.H. Yin, S.L. Liu, C.L. Zhang, J.C. Bao, Y.L. Zheng, M. Han, Z.H. Dai, Well-coupled graphene and pd-based bimetallic nanocrystals nanocomposites for electrocatalytic oxygen reduction reaction, ACS Appl. Mater. INTERFACES 6 (3) (2014) 2086–2094.